© 2026 IEEE. Personal use of this material is permitted. Permission from IEEE must be obtained for all other uses, in any current or future media, including reprinting / republishing this material for advertising or promotional purposes, creating new collective works, for resale or redistribution to server or lists, or reuse of any copyrighted component of this work in other works.

Aging-Robust Precoding in Near-Field Cell-Free Massive MIMO with Mobile Multi-Antenna Users

Christian Simon Kamphus, Leonard Paul Schulz and Gerhard Bauch
Institute of Communications
Hamburg University of Technology
Hamburg, Germany
{christian.kamphus, leonard.schulz, bauch}@tuhh.de

***Abstract*—We propose a channel-aging-robust precoding scheme for multi-antenna users in a cell-free massive multiple-input multiple-output (MIMO) system operating at mmWave frequencies under line-of-sight (LoS) propagation. The proposed approach leverages instantaneous channel state information (CSI) at the receiver to compensate for outdated CSI at the transmitter, which arises due to user mobility and fronthaul latency in centralized architectures. To motivate the design, we analyze the spatial structure of the resulting near-field beampatterns formed by cooperating access points (APs) and show that their inherent periodicity can be exploited to obtain systematic spatial diversity gains at the multi-antenna users. We investigate the impact of user mobility on the downlink spectral efficiency and demonstrate that multi-antenna users can partially mitigate channel aging effects, particularly for small serving clusters. Numerical results reveal that the proposed approach reduces sensitivity to latency constraints and enables significant performance gains compared to a small-cell system under channel aging, reaching more than four times the 90%-likely per-user spectral efficiency in highly populated scenarios.**

***Index Terms*—Cell-free massive MIMO, near-field, mmWave communications, channel aging, spatial diversity, multi-antenna users**

I. Introduction

Cell-free massive multiple-input multiple-output (MIMO) has emerged as a promising paradigm for next-generation wireless networks, enabling dense deployments of distributed access points (APs) that jointly serve multiple user equipments (UEs) to improve coverage and reliability [1]. A wide range of cell-free architectures have been proposed, differing in their requirements on channel state information (CSI) availability and fronthaul signaling between APs and central processing units (CPUs) [2].

Most existing works on cell-free massive MIMO focus on sub-6 GHz frequency bands and assume block-fading Rayleigh channels without a line-of-sight (LoS) component [3]. However, at mmWave frequencies, LoS propagation becomes prevalent, and the channel behavior is largely determined by the underlying geometry of the network [4]. In this context, physically consistent channel models that explicitly capture the geometric relationship between APs and UEs become more relevant. A key aspect of such models is the distinction between far-field and near-field conditions. While individual antenna elements may operate in the far-field, large distributed arrays formed by cooperating APs can exhibit near-field characteristics [5], [6], [7]. This enables user separation not only in the angular domain but also in the range domain, increasing system degrees of freedom and improving user capacity [8].

Most current works on cell-free massive MIMO assume a block-fading channel, where the channel realization is considered constant within a coherence block. In practice, user mobility leads to continuously evolving channels, resulting in the so-called channel aging effect. In this case, CSI becomes outdated over time while remaining temporally correlated. The impact of channel aging has been characterized in cell-free massive MIMO systems in [9], [10]. The performance of a near-field cell-free massive MIMO system considering Rician fading with channel aging was investigated in [11].

Furthermore, most prior works assume single-antenna users, despite the fact that modern devices are typically equipped with multiple antennas. Current mid-band 5G devices commonly employ four antennas, and even larger antenna arrays are expected in 6G devices operating at higher frequencies. While some recent studies have considered multi-antenna users in cell-free massive MIMO systems (e.g., [12]), they mostly neglect the impact of channel aging.

In this paper, we consider mobility in a mmWave system, where the short channel coherence times caused by user mobility lead to rapidly outdated CSI at the APs. In the downlink of centralized cell-free architectures, CSI must be collected from distributed APs, forwarded to a CPU, and used to compute and redistribute precoding vectors. This process introduces non-negligible fronthaul and computational latency, which becomes particularly critical at mmWave frequencies due to increased Doppler shifts and reduced coherence times.

We exploit multi-antenna users with instantaneous CSI to compensate for outdated transmitter-side CSI by leveraging spatial diversity at the receiver. Building on this idea, we propose a channel-aging-robust precoding scheme that explicitly accounts for outdated CSI at the APs while enabling the UE to extract spatial diversity gains. This approach is motivated by the spatial structure of near-field-like beampatterns formed by cooperating APs, which we analyze to reveal systematic diversity opportunities.

We analyze the downlink performance of a cell-free massive MIMO system with multi-antenna users and APs under LoS propagation using the proposed precoder. For comparison, we also evaluate a corresponding small-cell system. In contrast to

This research was supported by the project 'Next Generation City Networking' (Grant No. 19DZ24004) at the Hanseatic Wireless Innovation Competence Center (HAWICC). The project is funded by the Federal Ministry of Transport via the German Center for Future Mobility (DZM).

cell-free systems, where coherent transmission across multiple distributed APs makes the system sensitive to phase errors caused by channel aging, small-cell systems under LoS propagation are significantly less affected, as their performance primarily depends on beam direction rather than precise phase alignment. Numerical results demonstrate that multi-antenna users can partially compensate for channel aging effects, particularly in configurations with small serving clusters, and highlight the influence of both cluster size and the number of user antennas on system performance. Overall, the proposed approach reduces the sensitivity of the system to channel aging and alleviates latency constraints.

II. System model

We consider a cell-free massive MIMO system consisting of L APs and K mobile multi-antenna UEs. Each AP has N antennas and each user has M antennas. The APs are connected to a CPU via fronthaul links. The UEs are assumed to move at a common speed v in different directions ϕ_k (according to Fig. 1), which affects the channel variations.

The communication is organized in resource blocks of τ_c time instants. In contrast to the conventional coherence block assumption, we consider a continuously evolving channel model within each resource block. At the nth time instant in an arbitrary block, the channel between AP l and UE k is denoted by $\mathbf{H}_{kl}[n] \in \mathbb{C}^{N\times M}$.

This paper focuses on downlink data transmission. At the beginning of each resource block, corresponding to time instant $n = 0$, the APs are assumed to have perfect channel knowledge and design the precoders based on this information. The precoders are then kept fixed over the τ_c time instants, while the channels evolve according to the mobility model. Moreover, each UE is assumed to have perfect knowledge of the effective downlink channels at every time instant.

We do not explicitly model pilot-based channel estimation to isolate the impact of channel aging. Hence, the derived spectral efficiency should be interpreted as an upper bound on the achievable performance. In practical systems, CSI is typically acquired at the APs via uplink pilots at the beginning of each resource block. Furthermore, downlink pilots need to be sent frequently within each resource block, typically once per channel coherence time, to estimate the instantaneous effective downlink channels. Since one data stream is transmitted per UE, one downlink pilot sequence would be assigned to each UE, analogous to uplink channel estimation.

A. Channel Model

We consider a free-space LoS channel between the k-th UE and the l-th AP. We assume that the UE array aperture and the displacement due to user movement within one resource block are on the order of several to tens of wavelengths and remain much smaller than the propagation distance between the AP and the UE, such that the far-field condition is satisfied. For example, in a cell-free massive MIMO system operating at 60 GHz, with λ_c denoting the signal wavelength, a maximum receive-region extent of $10\lambda_c$, accounting for both the UE array aperture and its displacement within one resource block, corresponds to a Rayleigh distance of $\frac{2\times(10\lambda_c)^2}{\lambda_c} = 1$ m, which

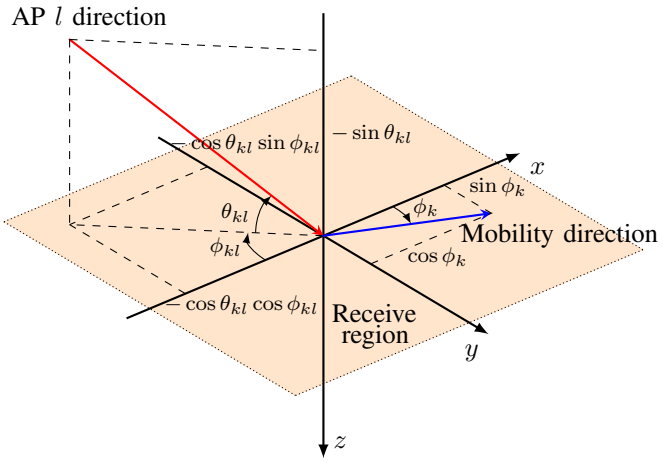


Fig. 1. Illustration of the coordinates and spatial angles for the receive region of UE k, similar to [13].

can easily be satisfied in practice due to the typical height difference between the AP and the UE. Thus, the plane-wave model can be used to describe the channel between each AP and UE. This implies that, within a resource block, the angles of departure (AoDs), angles of arrival (AoAs), and the amplitudes of the complex channel coefficients remain constant for each AP–UE link. Only the phase of each channel varies as the UE moves [13].

As shown in Fig. 1, the elevation and azimuth AoAs of the signals from the l-th AP at the k-th UE are denoted by $\theta_{kl} \in [-\pi/2, \pi/2]$ and $\phi_{kl} \in [-\pi, \pi]$, respectively. Based on geometric considerations, the difference in the signal propagation distance between the position (x_{km}, y_{km}) of the m-th receive antenna at UE k and the origin of the receive coordinate system is given by $\rho_{\mathrm{r},kl}(x_{km}, y_{km}) = x_{km}\cos\theta_{kl}\cos\phi_{kl} + y_{km}\cos\theta_{kl}\sin\phi_{kl}$. It implies that the channel response of the l-th AP at the m-th receive antenna at UE k exhibits a $2\pi\rho_{\mathrm{r},kl}(x_{km}, y_{km})/\lambda_c$ phase difference with respect to the origin. To account for such phase differences in all M receive antennas at UE k, the array response vector of UE k with respect to AP l is defined as

$$\mathbf{a}_{\mathrm{r},kl} = [e^{j\frac{2\pi}{\lambda_c}\rho_{\mathrm{r},kl}(x_{k1},y_{k1})}, ..., e^{j\frac{2\pi}{\lambda_c}\rho_{\mathrm{r},kl}(x_{kM},y_{kM})}]^{\mathrm{T}}. \quad (1)$$

Similarly, for any antenna position (x_{ln}, y_{ln}) at AP l, the array response vector is defined as

$$\mathbf{a}_{\mathrm{t},kl} = [e^{j\frac{2\pi}{\lambda_c}\rho_{\mathrm{t},kl}(x_{l1},y_{l1})}, ..., e^{j\frac{2\pi}{\lambda_c}\rho_{\mathrm{t},kl}(x_{lN},y_{lN})}]^{\mathrm{T}}, \quad (2)$$

where $\rho_{\mathrm{t},kl}(x_{ln}, y_{ln})$ is the difference of the signal propagation distance at the n-th antenna at AP l. As a result, the free-space LoS channel matrix between the k-th UE and the l-th AP is obtained as

$$\mathbf{H}_{kl} = \sigma_{kl}\mathbf{a}_{\mathrm{t},kl}\mathbf{a}_{\mathrm{r},kl}^{\mathrm{H}}, \quad (3)$$

where $\sigma_{kl} = \frac{\lambda_c}{4\pi d_{kl}}e^{-j\frac{2\pi}{\lambda_c}d_{kl}}$ and d_{kl} is the distance between AP l and UE k.

B. Channel Aging

The relative movements between the UEs and APs lead to temporal variations in the propagation environment which affect the channel coefficients within a resource block. The channel realization $\mathbf{H}_{kl}[n]$ can be modeled as a function of its

initial state $\mathbf{H}_{kl}[0]$ and a phase shift due to the Doppler shift $f_{\mathrm{D},kl}$, such as

$$\mathbf{H}_{kl}[n] = \mathbf{H}_{kl}[0]e^{-j2\pi f_{\mathrm{D},kl}T_{\mathrm{s}}n}, \quad n = 0, 1, ..., \tau_c - 1, \quad (4)$$

where T_{s} denotes the sampling time. The Doppler shift present in the link between AP l and UE k with velocity v is

$$f_{\mathrm{D},kl} = \frac{v}{\lambda_{\mathrm{c}}} \cos\theta_{kl} \cos(\phi_k - \phi_{kl}). \quad (5)$$

C. Downlink Data Transmission

To model which APs serve which UEs, we define a set of diagonal matrices $\mathbf{D}_{kl} \in \mathbb{C}^{N\times N}$, for $k = 1, ..., K$ and $l = 1, ..., L$. More precisely, $\mathbf{D}_{kl}$ is the identity matrix $\mathbf{I}_N$ if AP l is allowed to transmit signals to UE k and $\mathbf{0}_{N\times N}$ otherwise. Moreover, we stack all the $\mathbf{D}_{kl}$ matrices diagonally to obtain $\mathbf{D}_k = \mathrm{diag}(\mathbf{D}_{k1}, ..., \mathbf{D}_{kL}) \in \mathbb{C}^{LN\times LN}$. Each UE is associated with the same fixed number of APs corresponding to the largest values of the large-scale channel gains $\beta_{kl} = |\sigma_{kl}|^2$.

We consider single-data stream transmission per user. To obtain a convenient notation similar to [12], we stack all the AP channels to UE k in the $LN \times M$ matrix $\mathbf{H}_k[n] = [\mathbf{H}_{k1}^{\mathrm{T}}[n], ..., \mathbf{H}_{kL}^{\mathrm{T}}[n]]^{\mathrm{T}}$. Furthermore, we denote the precoding vector of UE k designed based on the CSI at time instant $n = 0$ as $\mathbf{w}_k = [\mathbf{w}_{k1}^{\mathrm{T}}, ..., \mathbf{w}_{kL}^{\mathrm{T}}]^{\mathrm{T}} \in \mathbb{C}^{LN}$, where $\mathbf{w}_{kl} \in \mathbb{C}^N$ is the part used by AP l. Hence, the transmitted data signal $\mathbf{x}_{kl}[n] \in \mathbb{C}^N$ from AP l meant for UE k is $\mathbf{x}_{kl}[n] = \mathbf{D}_{kl}\mathbf{w}_{kl}\varsigma_k[n]$, where $\varsigma_k[n] \sim \mathcal{NC}(0, 1)$ is the data signal. The precoding vectors can be chosen arbitrarily such that $\mathbb{E}\left\{\|\mathbf{x}_l[n]\|^2\right\} = \sum_{i=1}^K \mathbb{E}\left\{\|\mathbf{D}_{il}\mathbf{w}_{il}\|^2\right\} \leq \rho_d$, where ρ_d is the maximum transmit power and $\mathbf{x}_l[n] = \sum_{i=1}^K \mathbf{x}_{il}[n]$ is the sum of all transmitted signals from AP l.

The received signal $\mathbf{y}_k[n]$ at UE k during the instants $0 \leq n < \tau_c$ is then given by

$$\mathbf{y}_k[n] = \mathbf{H}_k^{\mathrm{H}}[n]\mathbf{D}_k\mathbf{w}_k\varsigma_k[n] + \sum_{i=1, i\neq k}^{K} \mathbf{H}_k^{\mathrm{H}}[n]\mathbf{D}_i\mathbf{w}_i\varsigma_i[n] + \mathbf{n}_k[n], \quad (6)$$

where $\mathbf{n}_k[n] \sim \mathcal{NC}(0, \mathbf{I}_M)$ is the normalized noise vector. The channel matrix and precoding vector appear in the form $\mathbf{b}_{ki}[n] = \mathbf{H}_k^{\mathrm{H}}[n]\mathbf{D}_i\mathbf{w}_i \in \mathbb{C}^M$ in (6). We will use this notation for the effective channel after precoding in the remainder of this paper.

D. Downlink Spectral Efficiency

We consider the ideal case with perfect channel knowledge of the effective channels at the receiver. In practice, the CSI needs to be measured by downlink pilots, which makes this case an upper bound. We write the downlink received signal in (6) as

$$\mathbf{y}_k[n] = \mathbf{b}_{kk}[n]\varsigma_k[n] + \mathbf{n}'_k[n], \quad (7)$$

where $\mathbf{n}'_k[n] = \sum_{i=1, i\neq k}^K \mathbf{H}_k^{\mathrm{H}}[n]\mathbf{D}_i\mathbf{w}_i\varsigma_i[n] + \mathbf{n}_k[n]$ is composed of the independent noise and interference terms. With perfect CSI at the UEs, an achievable SE at UE k is

$$\mathrm{SE}_k = \frac{1}{\tau_c}\sum_{n=0}^{\tau_c-1} \log_2\left(1 + \mathbf{b}_{kk}^{\mathrm{H}}[n]\boldsymbol{\Xi}_k^{-1}[n]\mathbf{b}_{kk}[n]\right), \quad (8)$$

where the covariance matrix $\boldsymbol{\Xi}_k[n] \in \mathbb{C}^{M\times M}$ of $\mathbf{n}'_k[n] \in \mathbb{C}^M$ is

$$\boldsymbol{\Xi}_k[n] = \mathbb{E}\left\{\mathbf{n}'_k[n]\mathbf{n}'^{\mathrm{H}}_k[n]\right\} = \sum_{i=1, i\neq k}^{K} \mathbf{b}_{ki}[n]\mathbf{b}_{ki}^{\mathrm{H}}[n] + \mathbf{I}_M.$$

This result is obtained by treating the term $\mathbf{n}'_k[n]$ as worst-case Gaussian noise, whitening the noise, and then stating the average SE with perfect CSI at the receiver [12].

III. Precoding Scheme

A. Beampattern Analysis

To design a channel-aging-robust precoding scheme, we analyze the spatial characteristics of the beampattern in the receive region of UE k (according to Fig. 1). For this analysis, we consider a simplified scenario with single-antenna APs located at the origin of the transmit coordinate system (i.e., $a_{\mathrm{t},kl} = 1$). The received signal at a position (x, y) in the receive region can then be expressed as

$$y_k(x, y) = \underbrace{\sum_{l=1}^{L} e^{j\frac{2\pi}{\lambda_{\mathrm{c}}}\rho_{\mathrm{r},kl}(x,y)} b_{kl}^k \varsigma_k}_{\text{Desired signal}} + \sum_{i=1, i\neq k}^{K} \underbrace{\sum_{l=1}^{L} e^{j\frac{2\pi}{\lambda_{\mathrm{c}}}\rho_{\mathrm{r},kl}(x,y)} b_{kl}^i \varsigma_i}_{\text{Interference signal } i} + n_k, \quad (9)$$

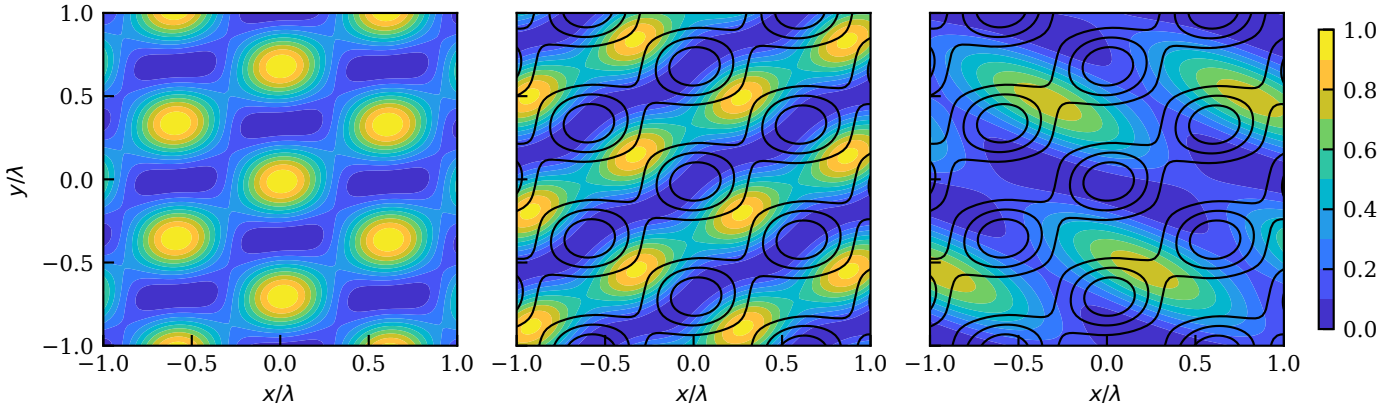
where $b_{kl}^i = \sigma_{kl}^* w_{il}$ is the effective channel from AP l to the receive region of UE k of the data signal i.

We analyze the beampattern in the receive region for given b_{kl}^i and AoAs θ_{kl}, ϕ_{kl}. An example of the beampattern of the desired signal for a UE served by three APs is shown in Fig. 2(a). The superposition of the three LoS components leads to a spatially periodic power distribution. The periodicity depends on the AoAs of the serving APs.

The essence of cell-free massive MIMO with single-antenna users is that the cooperating APs generate a small beam-focusing area at the user with a diameter of roughly half a wavelength [3]. However, under user mobility, the precoding has to be adjusted very frequently at mmWave frequencies, leading to stringent computational and fronthaul latency constraints. As an alternative, this paper motivates the use of multi-antenna users to achieve diversity gains from the periodic structure of the beampattern.

Fig. 2(b) shows the beampattern of the interference signal intended for a second UE in the receive region of the first UE, where both UEs are served by the same three APs. In this case, the first UE receives the interference signal from the same AoAs as for the desired signal. As a result, both signals exhibit the same spatial periodicity. The favorable positions with maximized SINR repeat across the receive region enabling systematic diversity gains.

Fig. 2(c) illustrates the case where the interfering UE is served by a cluster differing by one AP. This AP introduces a signal component with different AoA, which leads to a different spatial periodicity. In this case, the periodicity of the interference does not match that of the desired signal. This disrupts the periodicity of the maximum SINR positions.

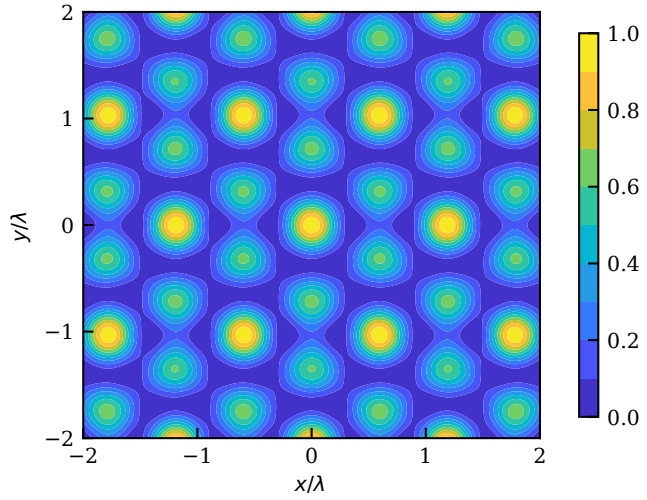


(a) Desired signal power
$b^1_{11} \approx 0.3, b^1_{12} \approx 0.2$
$b^1_{13} \approx 0.5, b^1_{14} = 0$

(b) Interference signal power (1)
$b^2_{11} \approx -0.4 - j0.2, b^2_{12} \approx 0.1 + j0.1$
$b^2_{13} \approx 0.3 + j0.2, b^2_{14} = 0$

(c) Interference signal power (2)
$b^3_{11} = 0, b^3_{12} \approx -0.2 - j0.3$
$b^3_{13} \approx 0.2 + j0.1, b^3_{14} \approx 0.2 + j0.2$

Fig. 2. Example of beampatterns of the desired signal resulting from three serving APs in (a), an interference signal resulting from the same serving AP set in (b) and an interference signal resulting from an AP set with one differing AP in (c). In (a) and (b) the AoAs are given by $\theta_{11} \approx \theta_{12} \approx \theta_{13} \approx 0.23, \phi_{11} \approx -\frac{\pi}{6}, \phi_{12} \approx -\frac{5}{6}\pi, \phi_{13} \approx \frac{\pi}{2}$. In (c), the 1st AP is excluded and the 4th AP with AoAs $\theta_{14} \approx 0.12$ and $\phi_{14} \approx \frac{5}{6}\pi$ is added. The black contour lines in (b) and (c) visualize the beampattern of the desired signal shown in (a).



$b^1_{11} \approx 0.284, b^1_{12} \approx 0.284$
$b^1_{13} \approx 0.284, b^1_{14} \approx 0.074, b^1_{15} \approx 0.074$

Fig. 3. Example of a beampattern of the desired signal resulting from five serving APs with AoAs $\theta_{11} \approx \theta_{12} \approx \theta_{13} \approx 0.23, \theta_{14} \approx \theta_{15} \approx 0.12, \phi_{11} \approx -\frac{\pi}{6}, \phi_{12} \approx -\frac{5}{6}\pi, \phi_{13} \approx \frac{\pi}{2}, \phi_{14} \approx \frac{5}{6}\pi, \phi_{15} \approx \frac{\pi}{6}$.

When the desired and interfering signals are generated by the same set of APs, they exhibit identical spatial periodicity. As a result, the spatial locations that provide favorable SINR conditions repeat systematically across the receive region. This creates multiple equivalent operating points that can be exploited by multi-antenna users for spatial diversity. In contrast, when the interfering signals originate from different AP sets, this periodic structure is not preserved.

In Fig. 3, a UE is served by five APs. The beampattern shows, in addition to global maxima, a large number of local maxima. Even though the larger number of serving APs generally leads to a larger coherent beamfocusing gain in the small beam-focusing area at $x = 0, y = 0$, the more pronounced small-scale fading in the spatial domain due to the local maxima requires larger receive arrays to achieve higher diversity gains under mobility.

B. Channel-Aging-Robust Partial MMSE Precoding Scheme

To design a precoder that is robust to channel aging, we build on the observations from Section III-A. In particular, only interference components that share the same set of serving APs and, thus, exhibit identical spatial periodicity as the desired signal, can be coherently suppressed. Here, coherent refers to phase-aligned superposition of the signals transmitted by the serving APs. As a result, the spatial locations that yield high SINR under coherent superposition repeat systematically across the receive region. In contrast, interference contributions from different AP sets do not preserve this structure and are therefore treated non-coherently.

To define our precoder, we introduce the selection vector $\mathbf{e}_k \in \mathbb{C}^M$, which selects one receive antenna used for precoder design. Since we consider single-stream transmission per user, $\mathbf{e}_k$ is a binary vector with a single non-zero entry. This reduces the CSI requirements at the transmitter while allowing the receiver to exploit the remaining dimensions for diversity. Consequently, we introduce the selected channel $\mathbf{h}_k[n] = \mathbf{H}_k[n]\mathbf{e}_k$, the used part of the channel $\widehat{\mathbf{h}}_k[n] = \mathbf{D}_k\mathbf{H}_k[n]\mathbf{e}_k$, which corresponds to the APs coherently serving UE k, and the unused part of the channel $\widetilde{\mathbf{h}}_k[n] = \mathbf{h}_k[n] - \widehat{\mathbf{h}}_k[n]$, which represents contributions from APs not serving UE k.

We propose an alternative partial MMSE precoder as

$$\overline{\mathbf{w}}_k = q_k \left(\sum_{i=1}^{K} q_i \mathbf{D}_k \left(\widehat{\mathbf{h}}_i[0]\widehat{\mathbf{h}}_i^{\mathrm{H}}[0] + \mathbf{C}_i \right) \mathbf{D}_k + \mathbf{I}_{LN} \right)^{-1} \widehat{\mathbf{h}}_k[0] \tag{10}$$

with channel covariance matrix $\mathbf{C}_i \in \mathbb{C}^{LN \times LN}$ of the unused channels and the transmit power q_i of UE i normalized by the noise power in the virtual uplink. We obtain the block diagonal matrix $\mathbf{C}_i = \mathrm{diag}(\mathbf{C}_{i1}, ..., \mathbf{C}_{iL})$, where each block is given by

$$\mathbf{C}_{il} = \mathbb{E}\left\{ \widetilde{\mathbf{h}}_{il}[n]\widetilde{\mathbf{h}}_{il}^{\mathrm{H}}[n] \right\}. \tag{11}$$

In contrast to conventional MMSE precoding, which assumes

coherent interference suppression across all APs, the proposed scheme explicitly accounts for the partial spatial consistency of the interference structure. The sum in (10) includes only the instantaneous channel components corresponding to APs that jointly serve both UEs (i.e., where $\mathbf{D}_k\mathbf{D}_i$ has ones). These components share the same AoAs and spatial periodicity and are therefore suppressed coherently. The channel covariance matrix models interference from APs that do not share the same spatial periodicity and are therefore treated non-coherently.

The per-AP power constraints, defined in Section II-C, must be satisfied. Hence, we normalize the precoders to UE k as

$$\mathbf{w}_k = \sqrt{\rho_k}\frac{\overline{\mathbf{w}}_k}{\sqrt{\mathbb{E}\left\{\|\overline{\mathbf{w}}_k\|^2\right\}}}, \tag{12}$$

where ρ_k determines how much power is allocated to UE k. In the numerical results, we consider

$$\rho_k = \rho_d \frac{\sqrt{\sum_{l\in\mathcal{M}_k}\beta_{kl}}}{\max\limits_{\ell\in\mathcal{M}_k}\sum_{i\in\mathcal{D}_\ell}\sqrt{\sum_{l\in\mathcal{M}_i}\beta_{il}}}, \tag{13}$$

where $\mathcal{M}_k \subset \{1,...,L\}$ denotes the subset of APs that serve UE k and $\mathcal{D}_l \subset \{1,...,K\}$ denotes the subset of UEs served by AP l. This slightly favors UEs with better channel conditions.

IV. Numerical Results

In this section, we present simulation results for a free-space road scenario to evaluate the performance of highly mobile vehicular UEs, as shown in Fig. 4. The road has a size of $2000\,\mathrm{m}\times 20\,\mathrm{m}$. The heights of the moving UEs ($v = 50\,\mathrm{km/h}$) are at $1.5\,\mathrm{m}$ with a random array orientation and mobility direction ϕ_k, each distributed as $\mathcal{U}(0, 2\pi)$, while the APs are placed at $10\,\mathrm{m}$. The APs are equally spaced along the road and the arrays are oriented towards the road. The antenna spacing is $\delta_0 = \lambda_c/2$ at the APs and UEs. The wraparound technique is applied at the ends of the road in the simulations to mimic an infinitely long road. We consider communication at the carrier frequency $f_c = 60\,\mathrm{GHz}$. The downlink transmission power is $P_d = 30\,\mathrm{dBm}$. The bandwidth is $B = 20\,\mathrm{MHz}$, and the noise power is $\sigma^2 = -96\,\mathrm{dBm}$. The length of one time instant is $T_s = 0.01\,\mathrm{ms}$. We assume that $L = 64, N = 8$ and $K = 128$ unless stated otherwise.

We compare the performance of a cell-free network with that of a corresponding small-cell network. We can treat the small-cell network as a degenerate case of a cell-free network where each UE is served by only one AP, that is, $|\mathcal{M}_k| = 1$. In the simulations, the APs and UEs in the small-cell setup are

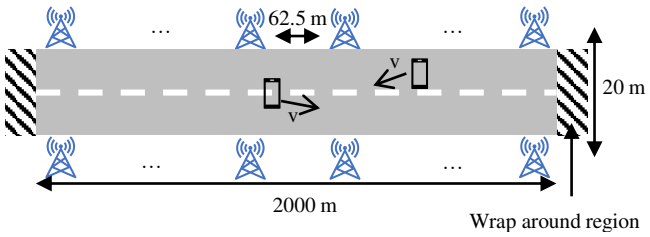


Fig. 4. Free-space road scenario with cell-free massive MIMO system (the fronthaul links and CPU are omitted in this figure).

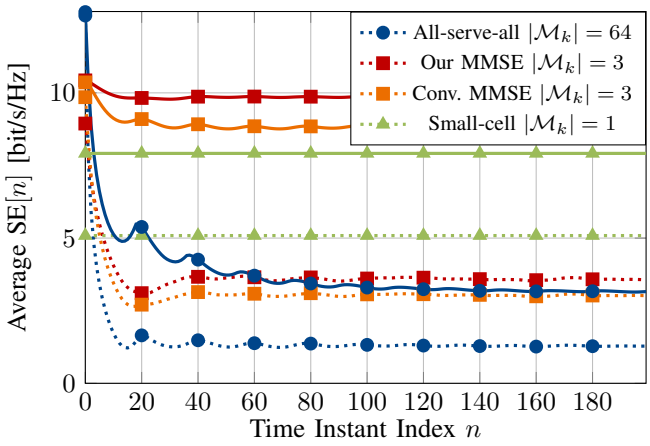


Fig. 5. Downlink average SE with time instant index for number of user antennas M and different cluster sizes $|\mathcal{M}_k|$. The solid lines represent UEs with $M = 4$ user antennas, while the dotted lines represent UEs with $M = 1$ user antennas.

deployed in the same locations and with the same number of antennas as in the cell-free network. We place the UEs so that each AP in the small-cell system serves the same number of UEs. Our simulations are implemented using Mimodium, an open-source cell-free massive MIMO simulation library [14].

A. Impact of the Number of Antennas per User

In Fig. 5, we show the downlink average SE$[n]$ (averaged over all UEs at time instant n) over the first 200 time instants for different cluster sizes and precoding schemes. The conventional MMSE precoder refers to a design that performs coherent interference suppression across all serving APs, without distinguishing between different spatial structures of the interference. For the all-serve-all and small-cell configurations, the proposed and conventional MMSE precoders coincide, such that both cases serve as common baselines.

At time instant $n = 0$, i.e., without channel aging, larger cluster sizes achieve higher SE due to increased beamforming gain. In particular, the all-serve-all case ($|\mathcal{M}_k| = 64$) provides the highest initial performance. However, as n increases, the performance of large clusters degrades rapidly due to the more pronounced spatial small-scale fading. In contrast, smaller cluster sizes exhibit significantly improved robustness against channel aging. For example, for $|\mathcal{M}_k| = 3$, the degradation over time is much less pronounced. As previously discussed, channel aging does not affect the small-cell scenario, since its performance does not rely on phase-aligned transmission across distributed APs.

Our proposed MMSE precoder shows improved robustness against channel aging compared to the conventional precoder. Since the interference is already partially mitigated by the directional beamforming of the APs, the degradation of the conventional precoder is less significant compared to the degradation of the cluster size. Our proposed precoder complements this by ensuring that interference is handled in a manner consistent with the underlying spatial structure identified in Section III-A.

Multi-antenna users significantly improve robustness by exploiting the spatial diversity induced by the periodic beam-

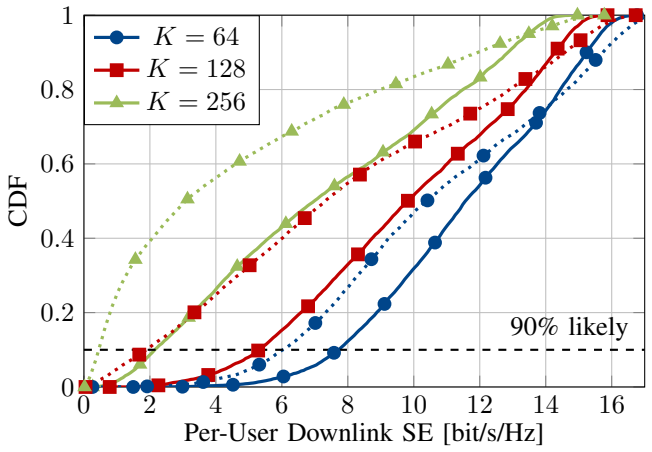


Fig. 6. CDF of per-user downlink SE for varying numbers of UEs with $M = 4$ antennas. The solid lines represent the cell-free setup with $|\mathcal{M}_k| = 3$, while the dotted lines represent the small-cell scenario (i.e., $|\mathcal{M}_k| = 1$).

pattern. However, the more APs serve a UE (i.e., the greater $|\mathcal{M}_k|$), the more receive antennas are required at the UE to achieve higher spatial diversity gains. For $M = 4$ and $|\mathcal{M}_k| = 3$, the average SE remains nearly constant over time, confirming that the system effectively leverages multiple favorable spatial locations as the user moves through the beampattern.

Similarly, the small-cell system also benefits from multi-antenna users due to the increased beamforming gain at the UE. However, as observed in Fig. 5, the cell-free system with $|\mathcal{M}_k| = 3$ and $M = 4$ provides both higher performance and robustness against channel aging.

B. Impact of the Number of Users

As the purpose of this paper is to evaluate performance over resource block lengths beyond several coherence blocks, we consider $\tau_c = 200$ in the following. We focus on the channel-aging-robust configurations identified in Fig. 5, namely the small-cell system and the cell-free system with $|\mathcal{M}_k| = 3$ and $M = 4$, for which the average SE$[n]$ remains approximately constant over time.

Fig. 6 shows the cumulative distribution function (CDF) of the per-user downlink SE for different numbers of UEs K. The cell-free system consistently outperforms the small-cell system in both the median and the 90%-likely SE. Moreover, the performance gap increases with the number of users. This behavior can be explained by the increased degrees of freedom in the cell-free system. In particular, the near-field propagation enables user separation not only in the angular domain but also in the range domain, which becomes increasingly beneficial as the user density grows. For $K = 256$, the cell-free system achieves more than four times the 90%-likely per-user SE compared to the corresponding small-cell system. Furthermore, the steeper CDF curves indicate a more uniform service quality among users, highlighting the improved fairness of the cell-free architecture even under channel aging.

V. Conclusions

In this paper, we analyzed the downlink performance of a cell-free massive MIMO system operating at mmWave frequencies under LoS propagation, explicitly accounting for channel aging and multi-antenna users. By examining the spatial characteristics of the resulting near-field-like beampatterns, we identified a periodic structure in the receive region that can be exploited to achieve systematic spatial diversity. Based on this insight, we proposed a channel-aging-robust precoding scheme that leverages multi-antenna users with instantaneous CSI to compensate for outdated transmitter-side CSI. Numerical results demonstrate that this approach effectively mitigates the degradation caused by channel aging, particularly in scenarios with small serving clusters. In addition, the proposed method reduces the sensitivity of the system to fronthaul and computational latency, which is critical in highly mobile mmWave deployments. Compared to a corresponding small-cell system, the considered cell-free architecture achieves significantly higher performance, especially in dense user scenarios. Future work may extend this framework by considering multiple spatial streams per UE, incorporating channel estimation, and evaluating the impact of pilot contamination.

References

[1] H. Q. Ngo, A. Ashikhmin, H. Yang, E. G. Larsson, and T. L. Marzetta, "Cell-Free Massive MIMO Versus Small Cells," *IEEE Transactions on Wireless Communications*, vol. 16, no. 3, pp. 1834–1850, Mar. 2017.

[2] E. Björnson and L. Sanguinetti, "Scalable Cell-Free Massive MIMO Systems," *IEEE Transactions on Communications*, vol. 68, no. 7, pp. 4247–4261, Jul. 2020.

[3] Ö. T. Demir, E. Björnson, and L. Sanguinetti, "Foundations of User-Centric Cell-Free Massive MIMO," *Foundations and Trends® in Signal Processing*, vol. 14, no. 3-4, pp. 162–472, 2021.

[4] A. N. Uwaechia and N. M. Mahyuddin, "A Comprehensive Survey on Millimeter Wave Communications for Fifth-Generation Wireless Networks: Feasibility and Challenges," *IEEE Access*, vol. 8, pp. 62 367–62 414, 2020.

[5] A. Kosasih, Ö. T. Demir, and E. Björnson, "Near-Field Beamfocusing, Localization, and Channel Estimation With Modular Linear Arrays," *IEEE Transactions on Wireless Communications*, vol. 25, pp. 8784–8798, 2026.

[6] M. Xie, X. Yu, J. Xu, B.-H. Soong, and C. Yuen, "Beam Focusing for Near-Field Cell-Free Massive MIMO," *IEEE Wireless Communications Letters*, vol. 14, no. 8, pp. 2491–2495, Aug. 2025.

[7] G. Mylonopoulos, G. Interdonato, S. Buzzi, and P. Liu, "Leveraging Line-of-Sight Propagation for Near-Field Beamfocusing in Cell-Free Networks," in *2025 33rd European Signal Processing Conference (EUSIPCO)*, Sep. 2025, pp. 1119–1123.

[8] Z. Wu and L. Dai, "Multiple Access for Near-Field Communications: SDMA or LDMA?" *IEEE Journal on Selected Areas in Communications*, vol. 41, no. 6, pp. 1918–1935, Jun. 2023.

[9] J. Zheng, J. Zhang, E. Björnson, and B. Ai, "Impact of Channel Aging on Cell-Free Massive MIMO Over Spatially Correlated Channels," *IEEE Transactions on Wireless Communications*, vol. 20, no. 10, pp. 6451–6466, Oct. 2021.

[10] H. Li, Y. Wang, C. Sun, and Z. Wang, "User-Centric Cell-Free Massive MIMO for IoT in Highly Dynamic Environments," *IEEE Internet of Things Journal*, vol. 11, no. 5, pp. 8658–8675, Mar. 2024.

[11] M. Xie, X. Yu, X. Dang, B.-H. Soong, and C. Yuen, "Near-Field Cell-Free Massive MIMO With Channel Aging: A Modified LoS Model," *IEEE Wireless Communications Letters*, vol. 13, no. 12, pp. 3553–3557, Dec. 2024.

[12] E. B. Kama, J. Kim, and E. Björnson, "Multi-Antenna Users in Cell-Free Massive MIMO: Stream Allocation and Necessity of Downlink Pilots," *IEEE Transactions on Communications*, vol. 74, pp. 2405–2419, 2026.

[13] L. Zhu, W. Ma, and R. Zhang, "Modeling and Performance Analysis for Movable Antenna Enabled Wireless Communications," *IEEE Transactions on Wireless Communications*, vol. 23, no. 6, pp. 6234–6250, Jun. 2024.

[14] L. P. Schulz, "Mimodium: Cell-Free Massive MIMO Simulation Library," Zenodo, Aug. 2026, doi: 10.5281/zenodo.22211988.